POLITECNICO DI TORINO
Repository ISTITUZIONALE

Validation of the GPM version-5 surface rainfall products over Great Britain and Ireland

Terms of use:

Publisher copyright

(Article begins on next page)

19 April 2024

SPECIAL
Global Precipitation Measurement (GPM)
COLLECTION

Validation of the GPM Version-5 Surface Rainfall Products over Great Britain and Ireland

DANIEL WATTERS

Earth Observation Science Group, Department of Physics and Astronomy, University of Leicester, Leicester, United Kingdom

ALESSANDRO BATTAGLIA

Earth Observation Science Group, Department of Physics and Astronomy, and National Centre for Earth Observation, University of Leicester, Leicester, United Kingdom

KAMIL MROZ

National Centre for Earth Observation, University of Leicester, Leicester, United Kingdom

FRÉDÉRIC TRIDON

Earth Observation Science Group, Department of Physics and Astronomy, University of Leicester, Leicester, United Kingdom

(Manuscript received 15 March 2018, in final form 29 August 2018)

ABSTRACT

Instantaneous surface rain rate estimates from the Global Precipitation Measurement (GPM) mission's Dual-Frequency Precipitation Radar (DPR) and combined DPR and multifrequency microwave imager (CMB) version-5 products are compared to those from the Met Office Radarnet 4 system's Great Britain and Ireland (GBI) radar composite product. The spaceborne and ground-based rainfall products are collocated spatially and temporally and compared at 5- and 25-km resolutions over GBI during a 3-yr period (from May 2014 to April 2017). The comparison results are evaluated as a function of both the intensity and variability of precipitation within the DPR field of view and are stratified spatially and seasonally. CMB and DPR products underestimate rain rates with respect to the Radarnet product by 21% and 31%, respectively, when considering 25-km resolution data taken within 75 km of a ground-based radar. Large variability in the discrepancies between spaceborne and ground-based rain rate estimates is the result of limitations of both systems and random errors in the collocation of their measurements. The Radarnet retrieval is affected by issues with measuring the vertical extent of precipitation at far ranges, while the GPM system struggles in properly quantifying orographic precipitation. Part of the underestimation by the GPM products appears to be a consequence of an erroneous DPR clutter identification in the presence of low freezing levels. Both products are susceptible to seasonal variations in performance and decreases in precision with increased levels of heterogeneity within the instruments' field of view.

1. Introduction

The Global Precipitation Measurement *Core Observatory* (GPM *CO*) satellite, launched in February 2014, offers unprecedented spaceborne observations of the three-dimensional structure of precipitating systems (Hou et al. 2014). The satellite detects rain rates in the range 0.2–110.0 mm h^{-1} and travels in a sun-asynchronous orbit, providing coverage between 68°N and 68°S, thus augmenting the 37°N/S coverage of the predecessor Tropical Rainfall Measuring Mission (TRMM) satellite (Skofronick-Jackson et al. 2017, 2018; Hou et al. 2014; Simpson et al. 1996). The GPM *CO* is complementing a

⌀ Denotes content that is immediately available upon publication as open access.

Corresponding author: Daniel Watters, dcw17@leicester.ac.uk

constellation of satellites with microwave radiometers, which together cover over 90% of Earth's surface and enact the philosophy of the GPM mission by providing global precipitation data from a calibrated system. Such an integrated observing system has the potential to greatly enhance our understanding of the global hydrological cycle and, thanks to the short latency of the precipitation products, can currently be used for a wide variety of applications, such as disaster response, agricultural modeling, and monitoring of disease risks (Kirschbaum et al. 2017).

The GPM *CO* includes the Dual-Frequency Precipitation Radar (DPR) and a conically scanning multifrequency passive microwave radiometer [GPM Microwave Imager (GMI)] (Skofronick-Jackson et al. 2017). The DPR measures the three-dimensional structure of precipitation systems at Ka-band (35.5 GHz) and Ku-band (13.6 GHz) frequencies with vertical and horizontal resolutions of 250 m and 5 km, respectively. The Ku-band radar has a swath width of 245 km and a minimum detection threshold at nadir of 14.8 dBZ ($\sim$0.31 mm h^{-1}), while the Ka-band radar has slightly better sensitivity with a minimum detection threshold at nadir of 13.0 dBZ ($\sim$0.24 mm h^{-1}, when operating in the high sensitivity mode) but a narrow swath width of 120 km (T. Iguchi 2018, personal communication). The GMI operates at 13 channels with frequencies between 10 and 183 GHz and has the highest spatial resolution of any radiometer within the GPM satellite constellation. The swath of the GMI (885 km) covers the DPR swaths, adding radiometric information to the radar measurements (Hou et al. 2014). Global precipitation data products from these GPM *CO* instruments are processed by both NASA's Precipitation Processing System (PPS) and JAXA's Mission Operations System (MOS). Level-2 instantaneous precipitation rates are produced using the DPR alone and with the GMI at the horizontal resolution of the DPR. According to the GPM mission science requirements for the data products, these products at 50 km × 50 km scale should have both a bias and random error of <50% for 1 mm h^{-1} and <25% for 10 mm h^{-1} (Skofronick-Jackson et al. 2016).

Satellite and ground-based radar measurements offer different benefits and limitations when sampling highly variable precipitation fields. Spaceborne radars provide global coverage but snapshot detections at different locations, whereas ground-based observations are paramount for a detailed understanding of regional precipitation by capturing the temporal variability of precipitation at a given location. However, ground-based radars must contend with range limits, beam blockage, and surface precipitation representativeness issues when sampling far above the surface at long ranges (Kidd et al. 2018). Spaceborne radars are less affected by mountain beam-blocking than ground-based systems (Wen et al. 2013), but tend to be more severely affected by signal attenuation due to their higher operating frequencies.

Comparison studies between precipitation occurrences and intensities from both perspectives can be very beneficial. Generally, gauge-adjusted ground-based radar measurements are referred to as "ground truth" and are used as a reference. The same approach is followed in this work with the Met Office radar rainfall estimates over Great Britain and Ireland (GBI), which are bias corrected using hourly gauge measurements (Fairman et al. 2015; Harrison et al. 1998).

Before the GPM era, several validation studies of TRMM products were conducted mainly over the continental United States. Kirstetter et al. (2012, 2013) and Bolen and Chandrasekar (2000) all found TRMM Precipitation Radar (PR) products to underestimate rain rates measured by U.S. ground-based radars. GPM validation studies have continued to use the continental U.S. test bed (Kidd et al. 2018; Chen and Chandrasekar 2016), though other studies have been conducted over Japan; Iguchi et al. (2016) compared Ku-band annual rainfall estimates from the GPM DPR to Automated Meteorological Data Acquisition System (AMeDAS) rain gauge data at 0.5° resolution, finding a DPR bias of −4.5%. However, this bias was found to be regionally variable with negative biases over land and positive biases over coastal areas.

Recently, a few studies have been conducted over Europe. Speirs et al. (2017) compared the GPM DPR level-2 version-4 rain rate product to a ground-based network of four dual-polarization C-band radars across Switzerland using the first two years of DPR measurements. The large range of topography due to the Swiss Alps and Plateau is ideal to test the precipitation estimates in complex terrain; they concluded the DPR performance to be superior in flatter terrain as well as in the summer due to a higher freezing altitude. Overall, GPM was found to underestimate precipitation amounts in comparison to the ground-based network with a bias of −39% and correlation of 0.643. Kidd et al. (2018) compared surface precipitation estimates from the GPM DPR (Ku band) and constellation of radiometers to those from ground-based radar and gauge networks over western Europe and the United States at 15-km resolution over a 3-yr period. The GPM constellation instruments were found to overpredict light precipitation occurrence and underestimate intermediate/ heavier rainfall over western Europe, while over the United States light precipitation overestimation was reduced and intermediate precipitation was overestimated.

Overall, most of the constellation instruments tend to underestimate rainfall intensities over both regions; the DPR and GMI products exhibited biases of -25% and -22% over western Europe and -4% and 15% over the United States, respectively. In particular, the GPM Ku-band radar and the GMI were found to exhibit among the strongest correlations over western Europe (0.49 and 0.53, respectively) and the United States (0.61 and 0.54, respectively).

This study validates the GPM DPR and DPR–GMI combined (CMB) version-5 rainfall products against the Radarnet 4 GBI composite product produced by the United Kingdom's Met Office. These two GPM products have reached a sufficient maturity for a thorough investigation. All of the other GPM products (including the constellation radiometer products and the IMERG products) are dependent upon the quality of these two cardinal products, and they lag one or two versions behind with regards to improvements. GBI is a perfect test bed for validation because it covers a midlatitude area including land (with varying orography, see Fig. 1), coastal, and oceanic regions. In particular, the region offers a different climatology to the locations of previous studies such as the United States: it is subject to fewer high-intensity events than the United States (Kidd et al. 2018), and precipitation occurrences mostly come from rain rates of less than $5\,\mathrm{mm\,h^{-1}}$ (Fairman et al. 2017). The light rain regime is particularly suited for assessing the minimum detection capabilities of the GPM *CO*.

This study collocates the ground reference 1-km-resolution Radarnet product to the 5-km-resolution DPR and CMB products during a 3-yr period, with the aim of assessing the quality of the products. Collocation of the products to a coarser 25-km resolution is also considered. Three years of GPM products offer the opportunity to consider seasonal and interannual variabilities. Furthermore, the fine horizontal resolution of the ground-observing system allows for an analysis of the effects of nonuniform beam filling (NUBF) on spaceborne measurements, which has been identified previously as a key problem with precipitation estimates from spaceborne radars (Kirstetter et al. 2015). Ultimately, this study helps to assess the capabilities of the GPM *CO* instruments to quantitatively estimate precipitation over various surfaces and orographies. The capabilities of individual GBI radars to contribute accurate measurements to the Radarnet product are also assessed.

Section 2 details the data products used from the GPM *CO* and the GBI radar network, methodology for collocation of the data products, and statistics for analysis. Section 3 presents the comparison results for 5- and 25-km resolution products, considering spatial, seasonal,
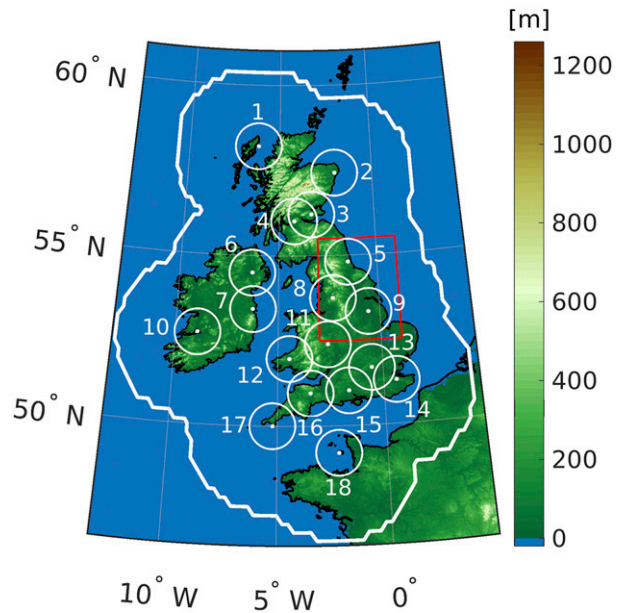

FIG. 1. The topography of GBI. The plot is made with data from Natural Earth. Each white dot represents the location of a ground-based radar that contributes to the Met Office Radarnet composite product. The radars are 1) Druim a'Starraig, 2) Hill of Dudwick, 3) Munduff Hill, 4) Holehead, 5) High Moorsley, 6) Castor Bay, 7) Dublin, 8) Hameldon Hill, 9) Ingham, 10) Shannon, 11) Clee Hill, 12) Crug-y-Gorllwyn, 13) Chenies, 14) Thurnham, 15) Dean Hill, 16) Cobbacombe Cross, 17) Predannack, and 18) Jersey. The white rings represent a 75-km range from each ground-based radar, the thick white contour represents the Radarnet composite extents, and the red box outlines the case study region shown in Fig. 2. Note that any region within the black coastlines is land, even though some inland regions may be blue as they reside below mean sea level.

rainfall intensity, NUBF, and clutter misclassification effects. In section 4, the results are discussed and some conclusions of the study are drawn.

2. Data and methodology

a. Data products

1) GPM *CO* DATA

The DPR and GMI observations are processed by the NASA PPS to produce the DPR-only product and the combined DPR and GMI product, which are stored as level-2A DPR and level-2B CMB data files, respectively, freely available from NASA (2017). The most recent version, version 5 (V05) released in May 2017, is used in this work. Level-2 data provide the precipitation rate at the surface plus additional parameters and flags, such as freezing-level altitude, range bin for the clutter-free bottom, and land surface type (ocean, land, coast,

inland water; Skofronick-Jackson et al. 2017). A description of the current and past GPM product versions can be found in Kidd et al. (2018). Details of the DPR and CMB rain profiling algorithms are described in Iguchi et al. (2017) and Olson et al. (2011), respectively.

Data within the DPR and CMB product files are provided at 5 km × 5 km resolution, across the DPR's swath (245 km, 49 rays per scan) and along the path of the GPM *CO*, providing continuous coverage. In this study, only data within the central 25 rays (120 km), known as the matched scan (MS) region where coincident measurements both at Ku band and Ka band are performed, are used. Within this data grid, the surface precipitation rates are used for each product (DPR, precipRateESurface; CMB, surfPrecipTotRate). Details of the data can be obtained from NASA (2014).

2) MET OFFICE RADAR NETWORK DATA

The Met Office radar network consists of 18 C-band frequency radars as shown in Fig. 1. The Radarnet composite surface rainfall product is produced every 5 min at 1-km horizontal resolution out to ~250-km range. With such range, the composite provides measurements over land, coastal, and oceanic regions. The Met Office Radarnet composite product is quality controlled and matches to within 2% of annual precipitation detected by surface rain gauges (Fairman et al. 2015). The time stamp on the composite data file represents the average of the end time of all individual radar scans. Radar scans that ended within 2 min before or 3 min after the composite data time contribute to the file (S. Best 2017, personal communication). These data can be acquired from the British Atmospheric Data Centre (BADC) upon request (Met Office 2003).

During the period of this study, the Met Office radar network was undergoing an upgrade to dual-polarization radars with potential benefits both in terms of improved rainfall estimates and data quality control. Each individual radar upgrade took ~6 months prior to operations returning again, though no two radars within the same region were upgraded at the same time to ensure that the composite measurements were not affected heavily. Of the 16 U.K. radars, 5 were upgraded prior to the study, 8 were upgraded during, and 3 were upgraded afterward. The 2 radars in Republic of Ireland were not upgraded as part of the scheme. More information on the polarimetric upgrades and time scales can be found at https://www.metoffice.gov.uk/services/industry/water/consultancy/radar-improvements-completion.

For the production of the composite data, each individual radar within the Met Office network produces up to eight low-elevation scans every 5 min

(Harrison et al. 2015) (15 min for the Dublin and Shannon radars; Fairman et al. 2015), at elevation angles between 0.5° and 4°. The scans provide reflectivity data with the best quality within 75-km range (Met Office 2009). Radar reflectivity measurements from each individual radar are subject to several quality control procedures, with details in Harrison et al. (1998, 2012, 2015) and Fairman et al. (2015). These procedures include the removal of noise, corrupt radar data, and anomalous propagation effects; accounting for beam blocking; and attenuation corrections. Rain rates R (mm h^{-1}) are deduced from the radar reflectivity factor Z (mm^6 m^{-3}) using a power law $Z = 200R^{1.6}$ (Marshall et al. 1955) for midlatitude stratiform rain, though the upgraded dual-polarization radars use the specific differential phase [based on a method from Beard and Chuang (1987)] to estimate high-intensity rain rates. Corrections for bright band, range, and orographic enhancement issues using idealized profiles of reflectivity (Kitchen et al. 1994) follow to deduce the corresponding surface rain rates, which are adjusted using hourly detections from rain gauges within 100 km of the radar. Once all corrections are made, measurements are gridded across GBI. Contributions to the composite grid are decided by using the measurement from the radar with the best quality index, which is a function of the measurement height of the lowest radar scan. As such, the nearest radar to a grid point will have the best quality index in most instances. The Met Office is currently working on using dual-polarization measurements to improve radar calibration. So far, polarimetry has aided Radarnet in identifying nonmeteorological returns (Harrison et al. 2015).

b. Collocation of data products

Several steps are taken in order to compare collocated instantaneous rain rates over GBI from the GPM *CO* and the Met Office radars. The rain rate pixels for all products are collocated temporally first and then spatially. The matching is performed at the location and time of each GPM DPR scan.

1) 5-KM RESOLUTION

The procedure follows that described in Mroz et al. (2017). First, the Radarnet 1-km data are temporally collocated to the GPM products. In the selected granules, the Radarnet rain rates are interpolated to each scan time of the DPR instrument over this region by producing a weighted mean (with no-rain measurements included) of the two closest 5-min-resolution Radarnet products. If Radarnet products are not available from within 5 min either side of the scan time, the whole granule is skipped. The temporal interpolation method

is used to better account for fast-moving and small-scale precipitation features in the comparison, rather than using a temporally closest product approach that can lead to temporal mismatches of up to 2.5 min. Afterward, the Radarnet product spatial resolution is reduced from 1 to 5 km by using a weighted mean of N Radarnet 1-km pixels within close vicinity of the center of each DPR 5-km pixel footprint, where the weighting corresponds to the two-way antenna gain ω_i of the DPR:

$$\omega_i = \exp\left[-\left(\frac{r_i}{2.5}\right)^2 \ln(4)\right], \tag{1}$$

where the index i corresponds to each 1-km Radarnet pixel close to the 5-km DPR pixel, and r_i is the distance in kilometers between the Radarnet 1-km pixel center location and the DPR bore-sight pointing location. The weighted Radarnet 5-km estimate corresponding to the DPR footprint location $\langle R_{\mathrm{RAD}}\rangle$ is calculated by

$$\langle R_{\mathrm{RAD}}\rangle = \frac{\sum_{i=1}^{N} \omega_i R_{\mathrm{RAD},i}}{\sum_{i=1}^{N} \omega_i}, \tag{2}$$

where $R_{\mathrm{RAD},i}$ is the rain rate estimate of the ith Radarnet 1-km pixel. The variability within each 5-km pixel footprint is also determined using the weighted sample standard deviation

$$\sigma_{\mathrm{footprint}} = \sqrt{\frac{V_1}{V_1^2 - V_2} \sum_{i=1}^{N} \omega_i (R_{\mathrm{RAD},i} - \langle R_{\mathrm{RAD}}\rangle)^2}, \tag{3}$$

where $V_1 = \sum_{i=1}^{N} \omega_i$ and $V_2 = \sum_{i=1}^{N} \omega_i^2$, as used by Kirstetter et al. (2012).

Two criteria, similar to those assigned by Kirstetter et al. (2012), are applied to quality control the number of Radarnet 5-km pixels for use in the validation: 1) pixels where >20% of the Radarnet 1-km data are missing are excluded and 2) a minimum of 16 Radarnet 1-km pixels within the 2.5-km radius of the 5-km pixel center is required. Any GPM product pixels that are collocated with the discarded Radarnet 5-km pixels are also removed prior to the comparison, and the remaining pixels are referred to as quality-controlled henceforth. These constraints ensure that only representative 5-km pixels are used and allow for a balanced assessment of the NUBF within the GPM 5-km pixels.

2) 25-KM RESOLUTION

The GPM and Radarnet products are also averaged at the 25-km scale to mitigate for possible collocation issues. The 25-km pixels are selected by taking 5 × 5

adjacent DPR pixels. A simple mean of the 5-km pixels within the larger pixel is used for calculating rain intensities; in the case of the surface-type flag, the flag that dominates ≥90% of the 25-km pixel is used. If no surface-type flag dominates the 25-km pixel, the pixel is excluded from the surface-type analysis but remains in the overall analysis. The 25-km pixels are subject to quality control prior to use in the validation: 1) all 5-km pixels used in the production of the 25-km pixel must obey the first 5-km-resolution quality criterion; 2) to mirror the second criterion for the 5-km quality control, each 25-km pixel must comprise at least 400 Radarnet 1-km pixels (i.e., 16 Radarnet 1-km pixels per 5-km pixel on average).

3) CASE STUDY

An intense precipitation event, as captured by the Met Office radar network and the GPM CO, over a region of GBI on 21 November 2016, is depicted in Fig. 2. Figures 2a and 2b exhibit the Radarnet product at its native resolution and resampled to the GPM resolution, respectively. Furthermore, NUBF values from Fig. 2c [refer to section 2c(2) for more information] suggest that the largest inhomogeneity at the 5-km scale exists on the storm outskirts where the rain rates are very low, whereas more homogeneous rain rates are distributed within regions where intensities surpass 1 mm h^{-1}. The DPR and CMB products at 5-km resolution are shown in Figs. 2d and 2e, and the difference between these products and the Radarnet product are shown in Figs. 2g and 2h, respectively. Generally, the Radarnet product provides low rain rate estimates over the ocean compared to the GPM products, and though the intense event over land is captured by all products, the GPM products fail to represent its variability and intensity. Brightness temperatures measured by the GMI at 37 and 89 GHz are shown in Figs. 2f and 2i. Rainfall over the ocean is evident in the 37-GHz channel from its emission effects against the cold background, whereas over land the storm is clearly identified by 89-GHz scattering signatures. Figure 3 depicts the along-track vertical cross sections of reflectivity measured at both the DPR Ku-band and Ka-band channels corresponding to the magenta/yellow outlined box in Figs. 2b–e, 2g, and 2h. For this case study, the freezing level (magenta line) resides just below 2-km altitude, with a melting layer producing a weak bright band below 2 km. The Ka-band has a worse sensitivity (18.7-dBZ minimum detection in matched scan mode, shown in Fig. 3b) than the Ku-band (14.8-dBZ minimum detection, shown in Fig. 3a) (T. Iguchi 2018, personal communication). Noticeably, some bins up to 2-km altitude and beyond are misclassified by the DPR algorithm as clutter, which then resides above the freezing level in early scans.
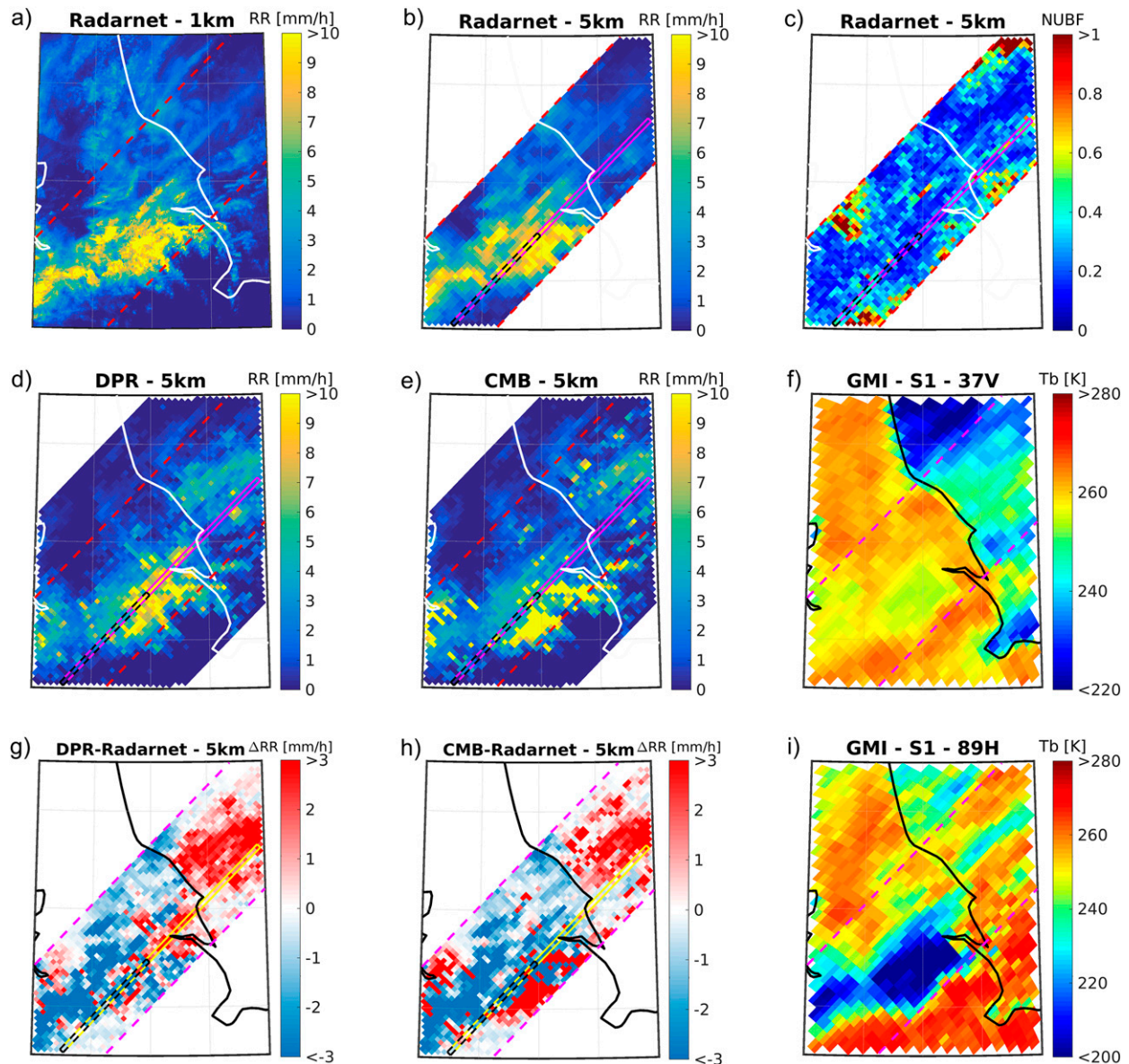
FIG. 2. (a) The 1-km-resolution Radarnet rain rate product, which has been interpolated to match the time stamp of the central GPM *CO* scan within the boxed region. (b) The 5-km-resolution collocated and quality-controlled Radarnet rain rate product. (c) The 5-km-resolution NUBF factor from the 1-km Radarnet rain rate product. (d) The 5-km-resolution DPR rain rate product. (e) The 5-km-resolution CMB rain rate product. (f) The 37-GHz vertical polarization and (i) 89-GHz horizontal polarization GMI brightness temperature product. Difference in 5-km-resolution rain rates (g) between the DPR product and the quality-controlled Radarnet product and (h) between the CMB product and the quality-controlled Radarnet product. The region between the dashed red lines in (a)–(e) and between the magenta lines in (f)–(i) represents the inner MS 120-km-wide swath of the DPR, within which collocation takes place. The pixels within the magenta box in (b)–(e) and the yellow box in (g) and (h) represent the rain rates from the CFBB shown in Fig. 3. The black dashed box in (b)–(e), (g), and (h) refers to the pixels where the rain rates are underestimated as a result of the clutter issues, with the vertical structure of these pixels shown in Fig. 3.

The cause appears to be due to the low melting layer and surface not being distinguished. This is important to the analysis as the surface rain rates from the DPR come from the clutter-free bottom bin (CFBB), and hence misclassifications of clutter result in underestimates of rain rates, as can be seen in Figs. 2g and 2h within the first several scans (see the black dashed box). All panels show the capabilities of all instruments used within the analysis to detect rainfall events, though key differences are seen between the rain rate products.
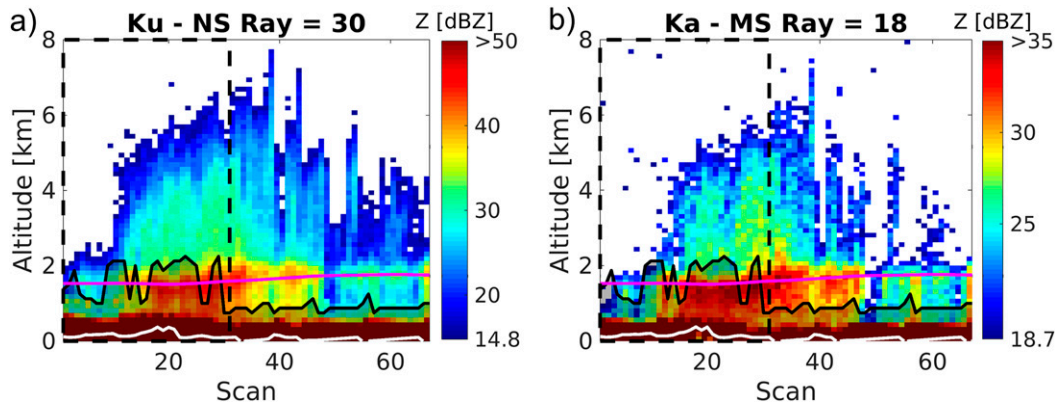
FIG. 3. (a) Ku measured reflectivity cut and (b) Ka (MS mode) measured reflectivity cut corresponding to the pixels within the magenta/yellow boxes in Figs. 2b–e, 2g, and 2h, where the black line is the CFBB defined by the DPR algorithm, and the shaded section below is clutter, the white line is the surface elevation, and the magenta line is the freezing level. Note that the detection thresholds at nadir for the Ku- and Ka-band (MS) reflectivities are 14.8 and 18.7 dB*Z*, respectively. The black dashed box refers to the pixels in Figs. 2b–e, 2g, and 2h, where the rain rates are underestimated as a result of the clutter issues. Note that the color bars differ for the Ku and Ka panels.

c. Statistical analysis

1) DATA SELECTION

Prior to a quantitative comparison of the rain rate products, the whole collocated dataset needs to be reduced to the pixels that can be confidently considered to be rainy as observed by both the ground-based and spaceborne systems. This can be done by applying different thresholds to the ground-based and spaceborne rain products and finding the values that maximize the Heidke skill score (HSS). Once these thresholds have been identified, the no-rain pixels can be discarded. Figure 4 shows an example of identifying the maximum HSS for the CMB product at 5-km resolution from a range of Radarnet and CMB rain–no rain thresholds. Previous data reduction techniques tend to apply the same rain–no rain threshold to both the satellite and ground-based datasets for the product comparison (Kidd et al. 2018; Speirs et al. 2017), for example, including using the prelaunch-defined DPR detection threshold of 0.2 mm h^{-1}. However, using such a threshold does not provide the maximum HSS (see the cross in Fig. 4). Meanwhile, using the maximum HSS (see the solid circle in Fig. 4) can also significantly reduce the number of pixels for the intercomparison. To avoid such inconvenience, in this study a DPR/CMB rain–no rain threshold that incorporates all positive rain rates is applied and, under this condition, the Radarnet rain–no rain threshold is found from the maximum HSS (referred to henceforth as the conditional maximum HSS; see the open circle in Fig. 4); this identifies the minimum Radarnet rain rate detected (but not necessarily accurately quantified) by the DPR/CMB algorithm. Setting

the DPR/CMB rain–no rain threshold so low may not enhance the number of useful pixels significantly at 5-km resolution, but it nearly doubles it at 25-km resolution. This has the advantage of providing more robust comparison statistics while keeping to within 0.03 of the overall maximum HSS, and hence the comparison statistics will not differ significantly from those computed using the thresholds of the overall maximum HSS.
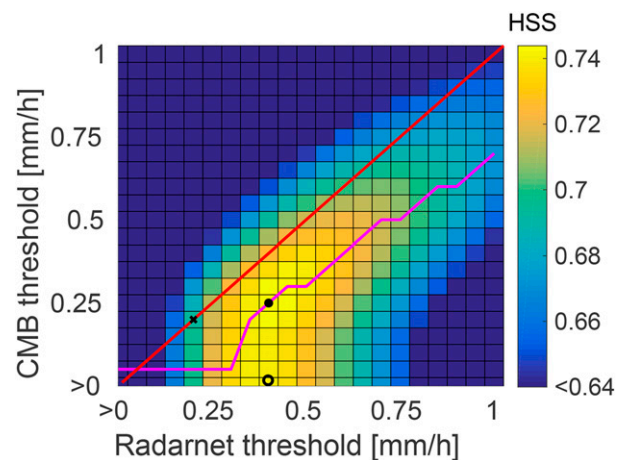

FIG. 4. HSS for the CMB product using the Radarnet product at 5-km resolution, as a function of the CMB rain–no rain threshold and the Radarnet rain–no rain threshold. Only rain rate estimates from within 75 km range of a ground-based radar are used. The solid circle identifies the thresholds with the maximum HSS, the cross identifies the thresholds used by Kidd et al. (2018), and the open circle represents the maximum HSS score when all positive CMB values are used and hence the down-selection thresholds of this study for the CMB–Radarnet comparison at 5-km resolution. The magenta line represents the CMB threshold that provides the maximum HSS score for each Radarnet threshold.

To find the Radarnet rain–no rain threshold that provides the conditional maximum HSS, several statistics are required. Hits h are determined to be measurements where GPM instruments and Met Office radars detected rain (i.e., measured at or above their respective rain–no rain thresholds). Misses m are measurements where the Met Office radars detected rain (i.e., measured at or above the Radarnet rain–no rain threshold) but the GPM instruments did not (i.e., measured below the DPR/CMB rain–no rain threshold). False detections f are measurements where GPM instruments detected rain but the Met Office radars did not. Correct rejections c are measurements where both the GPM instruments and the Met Office radars did not detect rain. From the number of measurements in each of these categories, three performance statistics are deduced. The probability of detection (POD) is the ratio of GPM rain detections to GPM and Met Office rain detections:

$$\text{POD} = \frac{h}{h+m}. \tag{4}$$

The false alarm ratio (FAR) assesses the fraction of GPM rain detections that are false:

$$\text{FAR} = \frac{f}{f+h}. \tag{5}$$

The HSS assesses how the instrument measurements compare to random estimates of rain rates and ranges between −1 and 1:

$$\text{HSS} = \frac{2(hc - fm)}{f^2 + m^2 + 2hc + (f+m)(h+c)}. \tag{6}$$

For the determination of the Radarnet rain–no rain threshold which provides the conditional maximum HSS, only measurements from within 75 km range of each ground-based radar are used so that the threshold is not affected by poorer-quality ground-based measurements at large distances. This study reveals that the conditional maximum HSS is obtained for a Radarnet rain–no rain threshold of 0.38 mm h^{-1} at 5-km resolution for both the DPR and CMB products. As the ground rain–no rain threshold that maximizes the HSS when considering all positive spaceborne rain rates can be regarded as the detection threshold of the spaceborne instrument (Kirstetter et al. 2015), this Radarnet rain–no rain threshold is treated hereafter as a sensitivity limit for the GPM platform over GBI. Similarly at 25-km resolution, a Radarnet rain–no rain threshold of 0.06 mm h^{-1} is found.

In summary, two conditions must be fulfilled for data entering further analysis: 1) the DPR/CMB algorithm estimates must be nonzero and 2) the Radarnet

estimates must exceed 0.38 mm h^{-1} at 5-km resolution and 0.06 mm h^{-1} at 25-km resolution. These data are henceforth referred to as the down-selected dataset. A period of 3 years is used to capture the interannual variability within the statistical comparison. Moreover, the analysis is clustered according to the surface type (land, ocean, coast) using the "landSurfaceType" flag from the DPR product.

The precipitation detection capabilities of the GPM CMB product at both resolutions using the GPM and Radarnet rain–no rain thresholds discussed are assessed in Table 1, which shows the POD, FAR, and HSS statistics (the statistics of the DPR product are similar and are not shown for brevity). Results are subset based on surface classification and the distance of the nearest ground-based radar. Coincident quality-controlled measurements from the CMB and Radarnet products are used. GPM instruments appear to detect around 72% of rain events beyond the DPR/CMB detection threshold at 5-km resolution, and 83% of rain events at 25-km resolution, with better detection capabilities over ocean than land and coastal regions. The fraction of false GPM rain measurements is 33% at 5-km resolution and 30% at 25-km resolution, with the least false alarms over land and most over the ocean. However, the marine false alarms are likely due to the ground-based radars missing rain events at far ranges. This is proven when considering data within 75 km of a ground radar, where FAR values are significantly reduced. All HSS scores are in the range of 0.64–0.79, with no particular surface-type consistently providing higher scores than the others. HSS values tend to improve when using data closer to ground-based radars, highlighting that range issues will have an effect on the comparison analysis.

2) COMPARISON STATISTICS

The normalized bias μ is

$$\mu = \frac{\sum_{k=1}^{n} \Delta R_k}{\sum_{k=1}^{n} R_{\text{RAD},k}} \times 100\%, \tag{7}$$

the normalized standard deviation σ is

$$\sigma = \frac{\sqrt{\dfrac{1}{n-1} \sum_{k=1}^{n} (\mu - \Delta R_k)^2}}{\dfrac{1}{n} \sum_{k=1}^{n} R_{\text{RAD},k}} \times 100\%, \tag{8}$$

and the correlation coefficients are the statistical quantities used to assess the difference between the two rainfall estimators within a comparison dataset. In Eqs. (7) and (8), n is the total number of averaged pixels, k is

TABLE 1. GPM detection capability statistics from the comparison of the CMB and Radarnet products, using the respective rain–no rain thresholds identified from the conditional HSS analysis provided in the text. Statistics for the DPR product are not shown as the values are very similar to those for the CMB product.

Satellite product	Data resolution	Surface classification	Vicinity of ground radar	POD	FAR	HSS
CMB V05	5 km	All	All	0.72	0.33	0.68
			<75 km	0.72	0.20	0.74
		Land	All	0.66	0.15	0.73
			<75 km	0.68	0.15	0.74
		Ocean	All	0.77	0.41	0.64
			<75 km	0.81	0.27	0.75
		Coast	All	0.69	0.18	0.73
			<75 km	0.70	0.19	0.73
CMB V05	25 km	All	All	0.83	0.30	0.71
			<75 km	0.80	0.16	0.77
		Land	All	0.77	0.14	0.78
			<75 km	0.77	0.11	0.79
		Ocean	All	0.87	0.40	0.65
			<75 km	0.85	0.25	0.75
		Coast	All	0.82	0.18	0.77
			<75 km	0.79	0.17	0.77

the spatially averaged pixel index, and $\Delta R_k = R_{\text{GPM},k} - R_{\text{RAD},k}$ is the difference in rain rates between the GPM ($R_{\text{GPM},k}$) and Radarnet ($R_{\text{RAD},k}$) products.

To characterize the inhomogeneity of the rainfall field within the 5-km footprint, the NUBF statistic:

$$\text{NUBF} = \frac{\sigma_{\text{footprint}}}{\langle R_{\text{RAD}} \rangle}, \qquad (9)$$

is used, as in Kirstetter et al. (2015).

3. Results

A detailed comparison of quality-controlled and down-selected instantaneous surface rain rate measurements from GPM and Radarnet products over the 3-yr period are carried out.

a. Statistical analysis

The comparison of the collocated GPM and Radarnet products from May 2014 to April 2017 are shown in Table 2 and Figs. 5 and 6. Probability density functions (PDFs) and cumulative density functions (CDFs) of precipitation for the different products at 5- and 25-km resolution are illustrated, prior to a direct comparison of the spaceborne and ground-based products on a pixel-by-pixel basis. Bias, standard deviation, and correlation are used, as defined in section 2c(2). Comparisons of the GPM data products against the Radarnet product are performed at different spatial scales (5 km, 25 km) for different surface types (all, land, ocean, coast) and for different measurement distances from the nearest ground-based radar (<5 km, or all distances within the composite range). Density scatterplots for rain rates

over all surfaces from measurements within 75 km of a ground-based radar at 5- and 25-km resolutions are presented in Fig. 6.

The PDFs and CDFs are depicted in Fig. 5, showing the DPR, CMB, and Radarnet down-selected data. By using down-selected Radarnet data, only 14% of the occurrence of original nonzero quality-controlled Radarnet rain rate estimates is preserved, though this equates to 74% of the rainfall volume. There are some quantitative differences at 25-km resolution, as 30% of the occurrence and 91% of the rainfall volume of original nonzero quality-controlled Radarnet rain rates estimates are preserved. At 5-km resolution, the peak occurrence of surface rain rates is $\sim 0.45 \, \text{mm h}^{-1}$ for the two GPM products, with both products exhibiting a decreasing function of rain rates beyond this intensity. A decreasing function of rain rates is also seen across all rain rates at 25-km resolution, though there is some disagreement between the products. Note that the DPR product favors more light rain than the CMB product at both scales. According to the Radarnet product at 5-km resolution, $\sim 40\%$ of detected occurrences within 5-km footprints are smaller than $1 \, \text{mm h}^{-1}$, but this corresponds to only $\sim 20\%$ of rainfall volume. On the other hand, $\sim 55\%$ of the total rain volume is attributed to rain rates greater than $2 \, \text{mm h}^{-1}$ though this equates to only $\sim 25\%$ of occurrences. At 25-km resolution, $\sim 80\%$ of detected Radarnet occurrences and $\sim 40\%$ of rainfall volume are smaller than $1 \, \text{mm h}^{-1}$. Approximately 30% of the total rain volume is attributed to rain rates greater than $2 \, \text{mm h}^{-1}$, though this equates to only $\sim 10\%$ of occurrences at the coarser scale. Rain rates above $10 \, \text{mm h}^{-1}$ are very rare at both resolutions.

TABLE 2. Statistical analysis results for the comparison of the GPM satellite products to the Radarnet ground-based product for different spatial averaging domains and using different data classifications.

Satellite product	Spatial averaging domain	Surface classification	Vicinity of ground radar	Sample	Bias (%)	Std dev (%)	Correlation
DPR V05	5 km	All	All	540 990	−21	127	0.41
			<75 km	145 945	−19	108	0.56
		Land	All	180 496	−32	127	0.39
			<75 km	84 978	−26	85	0.60
		Ocean	All	316 599	−12	127	0.43
			<75 km	46 195	−3	148	0.54
		Coast	All	43 770	−25	106	0.48
			<75 km	14 647	−18	114	0.57
DPR V05	25 km	All	All	60 622	−29	99	0.68
			<75 km	16 746	−31	77	0.79
		Land	All	12 716	−40	88	0.73
			<75 km	7035	−39	69	0.81
		Ocean	All	30 721	−19	111	0.64
			<75 km	3578	−14	91	0.79
		Coast	All	17 185	−37	85	0.73
			<75 km	6133	−31	78	0.78
CMB V05	5 km	All	All	544 487	−7	125	0.48
			<75 km	146 071	−6	110	0.60
		Land	All	181 881	−24	113	0.49
			<75 km	85 135	−16	102	0.59
		Ocean	All	318 325	7	133	0.50
			<75 km	46 160	17	126	0.64
		Coast	All	44 157	−18	110	0.50
			<75 km	14 652	−11	104	0.61
CMB V05	25 km	All	All	60 927	−17	102	0.68
			<75 km	16 852	−21	85	0.77
		Land	All	12 831	−33	86	0.75
			<75 km	7091	−30	76	0.78
		Ocean	All	30 811	0	118	0.66
			<75 km	3597	4	100	0.80
		Coast	All	17 285	−28	87	0.72
			<75 km	6164	−21	86	0.76

The pixel-by-pixel direct comparison of the spaceborne and ground-based products is provided in Table 2 and Fig. 6. The 5-km comparisons suggest that the DPR and CMB products underestimate rain rates with respect to Radarnet, with biases of −21% and −7%, respectively. For both products, large standard deviations of the difference between products (127% and 125%) and midrange correlations (0.41 and 0.48) suggest that the biases are highly variable at the 5-km scale. The CMB product is in better agreement with the Radarnet product according to smaller bias magnitude and slightly better correlation, and the reason for this is likely due to the additional information that the GMI provides on precipitation events. Large standard deviations for both GPM products can be partly attributed to random errors due to miscollocation.

The 25-km comparison presents larger underestimates of surface rain rates by the GPM products with respect to the Radarnet product, with biases of −29% and −17% for the DPR and CMB products respectively.

The purpose of the 25-km comparison is to use a spatial resolution that mitigates random errors associated with imperfect collocation at the DPR native resolution. As expected, the results at 25-km resolution are characterized by lower standard deviations and higher correlations than those at 5-km resolution. This is depicted in Fig. 6 by the smaller spread of data around the 1:1 line at the coarser resolution.

Measurements over ocean for both GPM products and spatial averaging domains tend to produce the smallest bias magnitude of all considered surface types. The improvement over ocean is likely due to GPM's improved performance as the uncertainty in path-integrated attenuation corrections tends to be less over ocean (Meneghini et al. 2015). On the other hand, land measurements produce the better standard deviations and correlations at 25-km scale. This could point toward a deficiency of Radarnet estimates over the ocean and better performance of the Met Office radars over land due to range effects.
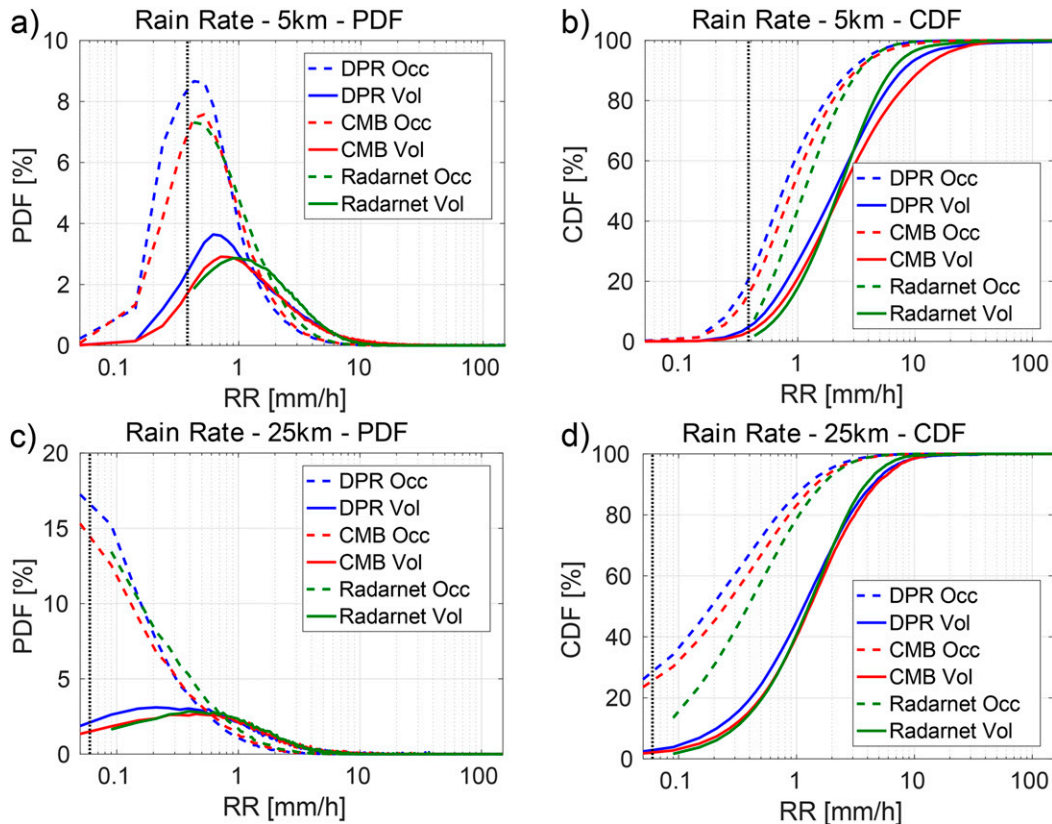
FIG. 5. The probability density functions of all instantaneous surface rain rate (RR) products at (a) 5- and (c) 25-km resolution. The cumulative density functions of all products at (b) 5- and (d) 25-km resolution. Dashed lines represent the occurrence (Occ) of rain rates, and solid lines represent the volume (Vol) of rain rates. The DPR, CMB, and Radarnet data are from the down-selected dataset identified as rainy by the criteria listed at the end of section 2c(1). The vertical black dotted lines correspond to the Radarnet rain–no rain threshold at the respective resolution (0.38 mm h^{-1} at 5-km resolution, 0.06 mm h^{-1} at 25-km resolution).

Overall, the GPM products tend to produce better statistics when considering 25-km measurements from within a 75-km radius of a ground-based radar. Large standard deviation and low correlation might be a result of the range deficiency of ground-based radars, as the lowest elevation scan-center height surpasses 2.6-km height above radar level beyond 150-km range from a ground-based radar (calculated taking into account Earth's curvature; Doviak and Zrnić 1993). For the following analysis, results will be considered in terms of these classifications unless otherwise stated (i.e., spatial, NUBF, and clutter analyses).

b. Spatial variability

Prior to spatially disaggregating the statistical results, average annual surface rainfall amounts measured by the Met Office ground-based radar network restricted to the GPM coincident scans are presented. The GPM *CO* overpasses GBI ~3–4 times per day with

a weak south–north gradient as a result of the GPM *CO*'s orbit. The rough estimates of the mean annual collocated rainfall amounts within 0.25° × 0.25° regions for the DPR, CMB, and Radarnet products are shown using 5-km resolution data which has not been subject to the down-selection procedure (i.e., all good measurements from a product within the 3-yr period), with the purpose of providing context to the following spatially stratified results. Data pixels are allocated into 0.25° × 0.25° bin if the location of their pixel center resides within the bin.

Figure 7 shows a gradient in accumulation from east to west over Great Britain, with the west coast receiving more rainfall amounts in agreement with previous results due to orographic enhancements (Fairman et al. 2017); on the other hand, both GPM products do not detect as strong a gradient in orographic enhancement or as much rainfall over the ocean though the CMB algorithm performs slightly better. The GPM products
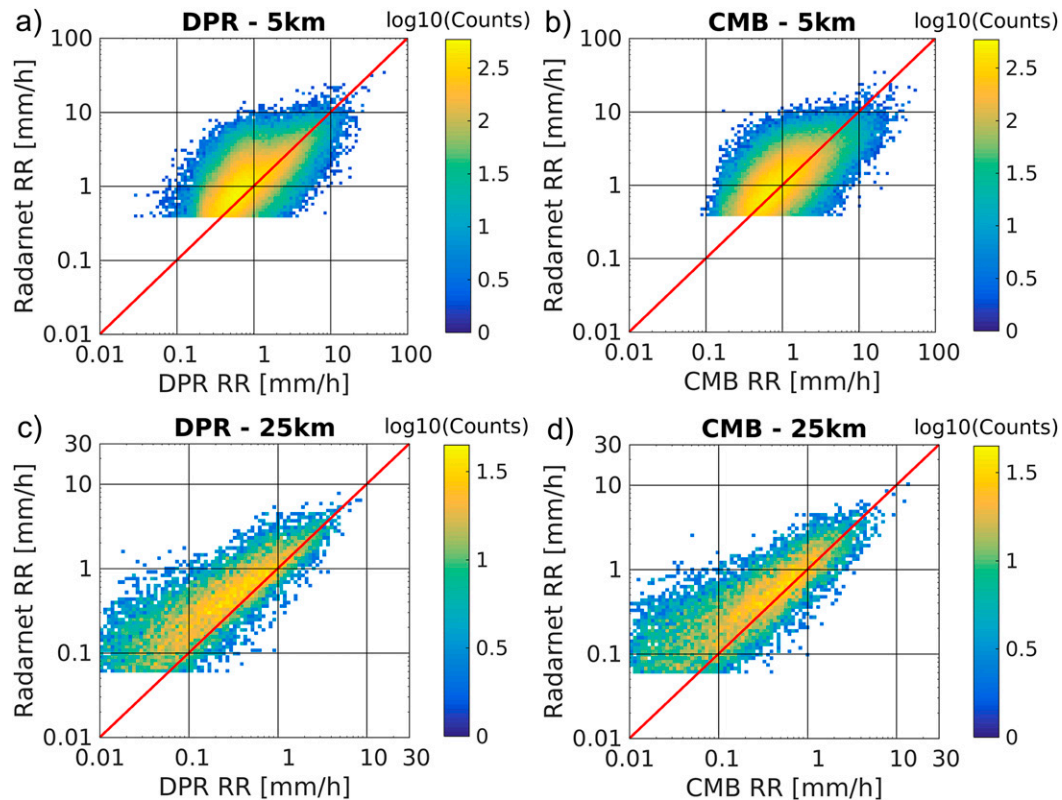
FIG. 6. Density scatterplots of GPM DPR and Radarnet surface rain rate (RR) products (from measurements within 75-km vicinity of a ground-based radar) collocated at (a) 5- and (c) 25-km resolution; GPM CMB and Radarnet surface rain rate products (from measurements within 75-km vicinity of a ground-radar) collocated at (b) 5- and (d) 25-km resolution.

better capture the rainfall amounts in nonorographic regions, such as the ocean and the southeast of England. Though the two GPM products tend to measure lesser rainfall amounts than the Radarnet product almost everywhere, they capture rainfall over the ocean better than the land. The GPM products only measure greater rainfall amounts at the edges of the Radarnet composite (~250-km range). The ground radars detect less rain near the composite edges, likely due to the radar beam overshooting shallow precipitation systems.

The comparison results are now disaggregated at the regional level with all collocated and down-selected 25-km pixels binned into 0.25° × 0.25° regions. The clustering of such pixels into 0.25° × 0.25° bins is chosen to understand the performance of the products at the regional scale, and to account for the GPM level-2 data not being gridded. The spatial variability of the statistical parameters (Fig. 8) is indicative of 1) different performances of the GPM algorithm over different surface types (e.g., land versus ocean, orography) and 2) anomalies of individual radars within the Met Office composite. In fact, GPM is expected to perform consistently over

homogeneous surface types, and so any regional discrepancies (in biases and standard deviations) must be the result of differences caused by individual ground-based radar behavior. The use of GPM as a calibrator for ground-based radars is proven in past research such as Warren et al. (2018). Since the nearest individual radar predominantly provides the rainfall estimate at each grid point in the composite Radarnet product, identification of miscalibrated ground-based radars is possible based upon differing statistics between ground-based radars when compared with GPM.

Spatial statistical results at 25-km resolution are shown in Fig. 8, with measurements within ~250 km from ground-based radars provided. The CMB product, rather than the DPR product, has been used due to its smaller bias magnitude in comparison to the Radarnet product. Furthermore, the spatial bias and standard deviation features do not differ significantly between the two products, with only more negative bias bins over ocean and smaller standard deviations for the DPR.

Evidently, there is a range issue with the ground-based radars. Within the 75-km range rings for each
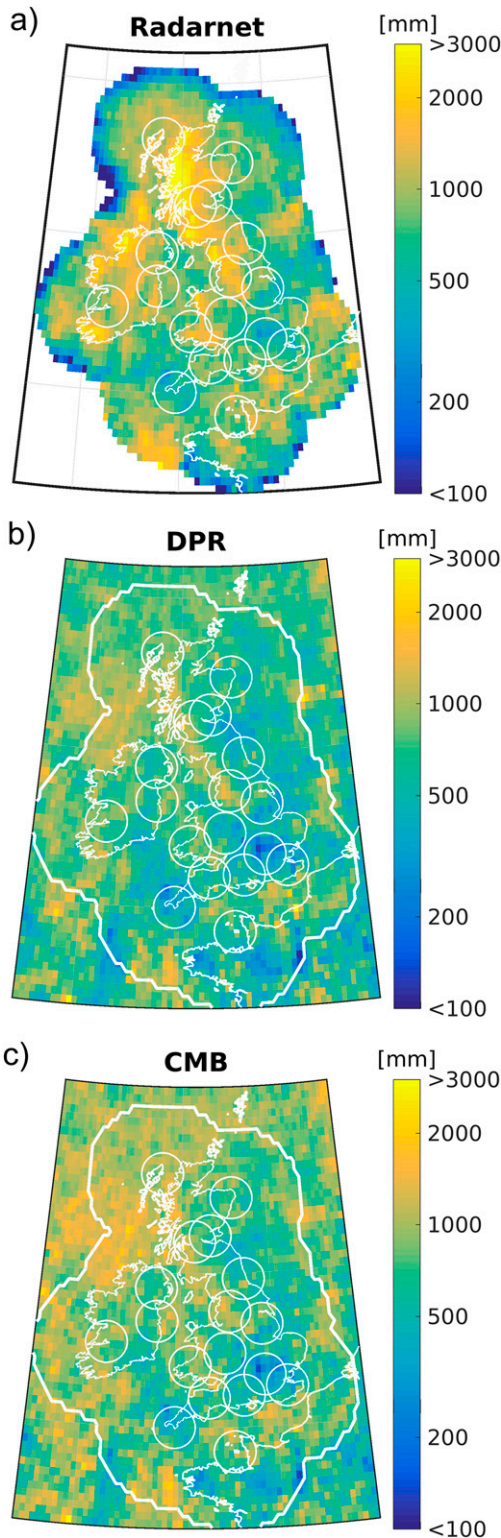
FIG. 7. Mean annual collocated rainfall amounts from (a) the Radarnet product, (b) the GPM DPR product, and (c) the GPM CMB product restricted to the GPM coincident scans. The 5-km resolution rain rates from each product are binned into 0.25° × 0.25° regions. The Radarnet data are quality-controlled, though the

radar, the biases are mostly negative (representing underestimation by the CMB product) as expected from Table 2. Furthermore, the standard deviations are relatively low. At ranges between ~150 and 250 km from each radar, this is not the case. These long-range measurements can predominantly be found over the ocean as any measurements over land are taken by multiple radars. At the bounds of the composite, the biases become positive (so the Radarnet product underestimates rain rates deduced by the CMB product) and the standard deviations become very large. These results suggest that there is high variability in the bias between satellite and ground-based radar measurements at long ranges, which implies that there are ground-based radar deficiencies in measuring surface rain rates at ranges beyond 150 km. In the first place, this range-based issue is driven by the large sampling altitude of ground-based radars at such long distances, with the corresponding issues related to vertical profile of reflectivity (VPR) extrapolations. In addition, due to the coarse resolution of the radar beam at far ranges, the radar beam may not be filled completely by precipitation, especially where the freezing level is low. This could result in underestimation of the rain rate for that bin and then underestimation of the ground rain rate after extrapolation using the idealized VPR in the Met Office correction scheme.

Noticeably, the CMB product underestimates rain rates compared to Radarnet at large distances for four radars, which differs from the overestimations for the other radars. These four radars are at the High Moorsley (radar 5 in Fig. 1, east coast of Britain), Thurnham (radar 14, southeast coast of Britain), Predannack (radar 17, southwest coast of Britain), and Jersey (radar 18, island north of France) sites. Warren (2014) found similar artifacts from the Jersey, High Moorsley, and Predannack radars when considering precipitation frequencies above $1 \, mm \, h^{-1}$ over a 5-yr period (2008–12), with these three radars found to have a pronounced maximum in rain occurrences at ranges of ~175–225 km, unlike the other radars. This behavior is puzzling and cannot be explained simply by a positive calibration bias; further investigation is needed to clarify this issue.

←

GPM and Radarnet data presented are not down-selected for comparison yet. The mean annual collocated amount is determined from the multiplication of the mean rain rate in a bin across the 3 years by $24 \, h \, day^{-1}$ and $365 \, days \, yr^{-1}$. As such, it is a rough estimate with which the differences between accumulations should be considered qualitatively. The rings represent a 75-km range from each ground-based radar, and the thick contour represents the Radarnet composite extents.
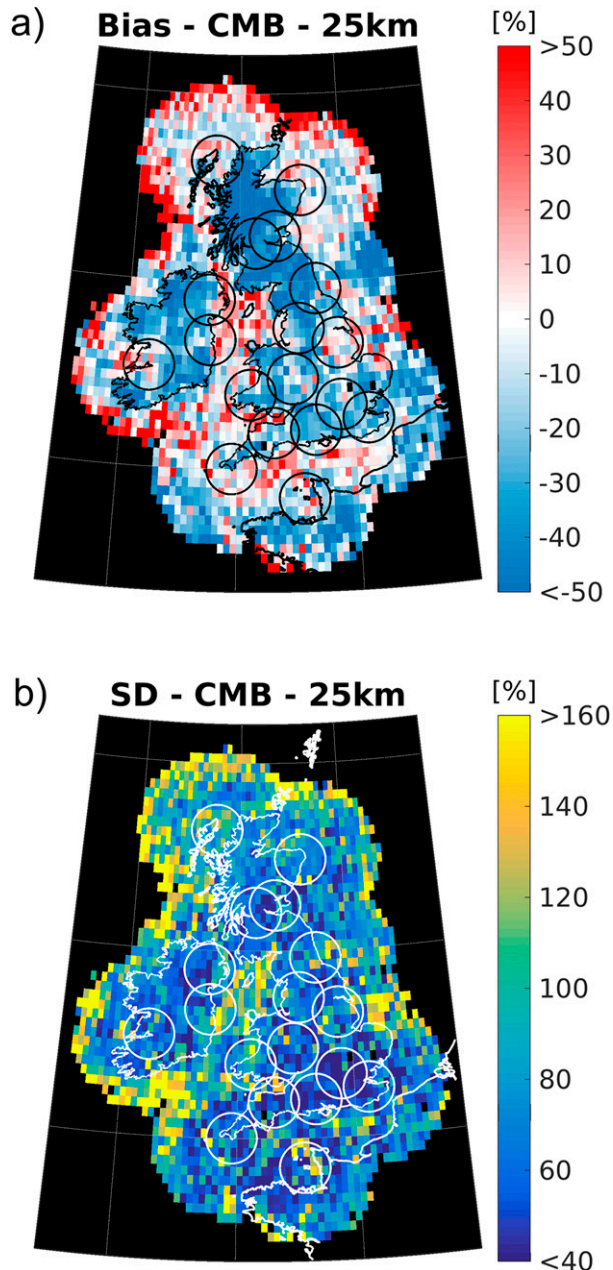
FIG. 8. (a) Regional normalized biases for the CMB–Radarnet products comparison, from 25-km resolution rain rates binned into 0.25° × 0.25° regions. (b) The regional normalized standard deviations (SDs) for the same respective products. Black bins represent those with less than 50% of the uniform number of measurements per bin (eight measurements), and the rings enclose bins within 75 km of a ground-based radar.

Predannack had undergone its polarimetric upgrades prior to this current analysis yet the range artifacts are still evident, though the reasons for this are currently unclear.

Finally, orographic effects clearly influence the discrepancy in rain rate measurements as GPM appears to underpredict surface rain rates to a greater extent over the west coast of Britain, as was shown in Fig. 7c. This implies two possibilities: 1) that the performance of GPM over mountainous regions is worse than over flatter regions as similarly concluded when Speirs et al. (2017) evaluated over Switzerland, or 2) that the ground-based radars overpredict surface rain rates in mountainous regions, which is possible because Harrison et al. (2012) suggests that there are uncertainties in the surface rain rates due to orographic effects and variations in the VPR. For Radarnet, the orographic enhancement for the idealized VPR was determined from only two separate case studies (Kitchen et al. 1994) and hence is uncertain and could lead to discrepancies between the actual rain rate at the surface and that deduced from the VPR. Future investigations into the efficacy of the VPR's orographic enhancement are required.

c. Seasonal and interannual variability

Seasonal trends in bias, standard deviation, and correlation are illustrated in Fig. 9. As found by Kidd et al. (2018) using 15-km pixels over Europe, there is clearly a seasonal trend in bias and correlation statistics for both GPM products, while a clear standard deviation trend is not identified. The results for 5-km pixels (not shown) are similar to those for the 25-km pixels. The most negative biases and lowest correlations occur during late winter and early spring, while the lowest magnitude biases and highest correlations are observed in the summer and early autumn. These features are likely associated with changes in the freezing level in different seasons: lower freezing levels during winter increase the difficulty of obtaining surface rainfall estimates from the ground-based radars and the spaceborne instruments. The Met Office radars are more likely to measure reflectivities above the melting layer in the winter, which introduces greater uncertainties in the VPR deduction of surface rain rate, while the GPM algorithm may misidentify the melting layer as clutter and provide a lower surface rate using a reflectivity above the melting layer (see Fig. 3). Notably, the CMB product always tends to have a smaller underestimating bias than the DPR product, suggesting better agreement with the Radarnet product across all seasons. The extents of the seasonal trend are similar in both products, though the DPR product shows slightly better standard deviation and correlation values.

d. Rainfall intensity variability

Normalized biases and standard deviations for the GPM products (with respect to the Radarnet product) are illustrated in Fig. 10 as a function of Radarnet
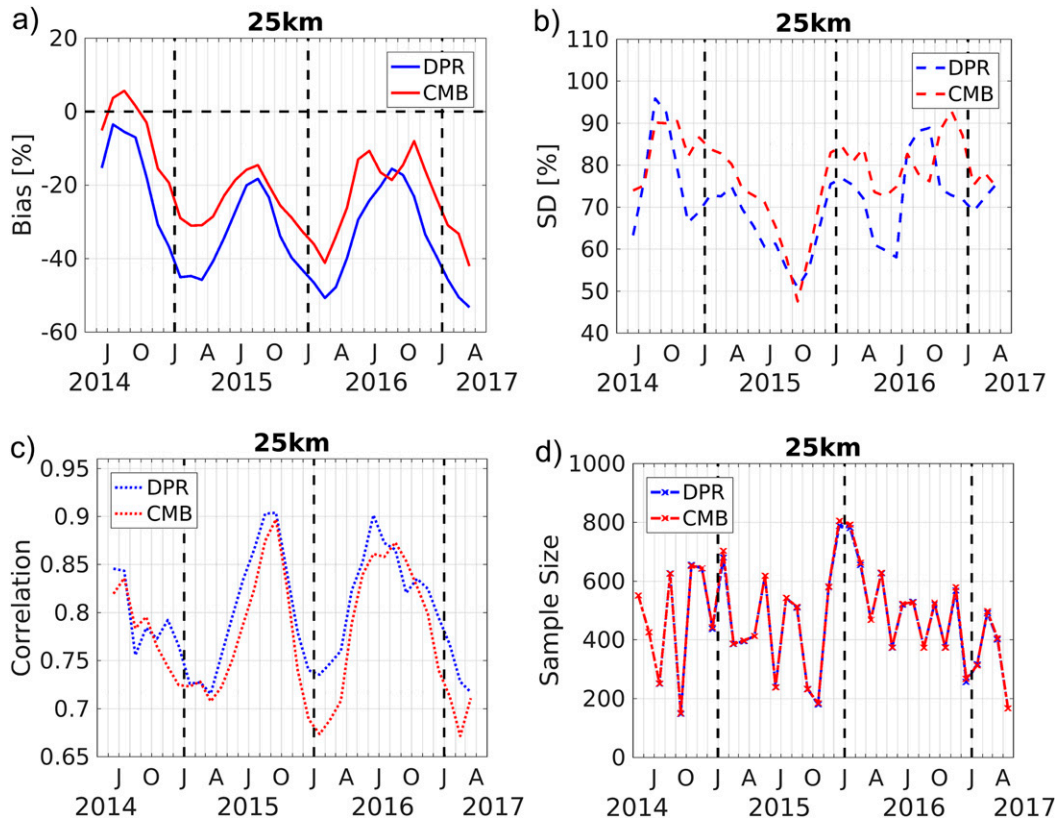
FIG. 9. (a) Monthly bias, (b) SD, (c) monthly correlation, and (d) monthly sample size of the GPM products with respect to the Radarnet product for 25-km resolution measurements, taken within 75-km of a ground-based radar. A 3-month convolution is used to smooth the data. Sample sizes for the DPR and CMB products are very similar, hence the CMB distribution overlies the DPR distribution. Note that the month labels are located at the first day of the corresponding month.

surface rain rates. This analysis helps in identifying rain rate regimes where the products perform optimally and where they suffer from large uncertainties. Moreover, the curves plotted in Fig. 10 can be compared with the GPM mission science requirements, which are defined for the interval between 1 and 10 mm h^{-1} and are represented by the green region.

At the 25-km scale, the CMB and DPR products clearly meet the mission requirements with regards to bias but slightly exceed them for standard deviation. The CMB product presents the better bias, but the DPR product has a smaller standard deviation, similar to what is found in Fig. 9. At 5-km resolution, the biases of the GPM products increase with increasing rain intensities from ~1 mm h^{-1}, and the DPR product only satisfies the mission requirements up to 5 mm h^{-1}. In fact, the DPR and CMB products overestimate rain rates below ~0.7 and 1.1 mm h^{-1} respectively, and underestimate them elsewhere. At 25-km resolution, the bias and standard deviation are relatively uniform across all rain rates with enhanced variability where there are low sample

numbers. These results are very encouraging as the requirements are expected to be met at a coarser 50-km resolution. Such resolution is not tested in this study as a result of the DPR's MS swath of 120 km: only two independent 50-km pixels would fit the swath width with a large associated reduction in sample size.

e. Nonuniform beam filling effects

Kirstetter et al. (2015) investigated NUBF effects by comparing the TRMM PR with the reference ground-based National Mosaic and Multi-Sensor Quantitative Precipitation Estimation (NMQ/Q2) product (i.e., gauge-adjusted radar data) over the contiguous United States and concluded that surface rain rate estimates from spaceborne instruments are affected by the rainfall variability within the footprint. Because of the similarity to its predecessor, GPM is likely to be affected by NUBF effects as well. The native Radarnet product at 1-km resolution allows for assessing the inhomogeneity within the 5-km DPR footprints. The effects of NUBF on bias and standard deviation statistics are shown in Fig. 11,
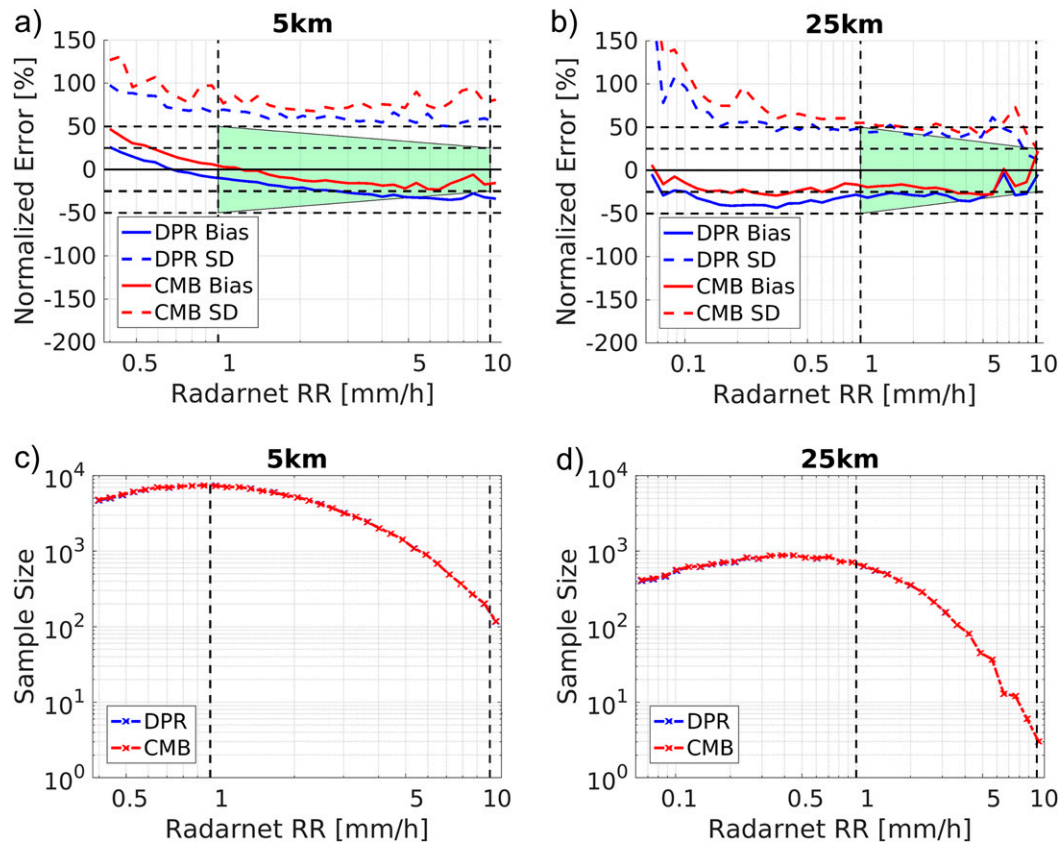
FIG. 10. Bias and SD of GPM products with respect to the Radarnet product as a function of Radarnet rain rates (RR) for (a) 5- and (b) 25-km-resolution measurements, taken within 75 km of a ground-based radar. Corresponding samples sizes at (c) 5- and (d) 25-km resolution are also shown. The green region represents the GPM mission science requirements at 50-km scale. Note that the horizontal axes differ in scale due to the differing downselection of data from different Radarnet rain–no rain thresholds at different resolutions. Sample sizes for the DPR and CMB products are very similar, hence the CMB distribution overlies the DPR distribution.

with only results from a sample of more than 100 pixels considered reliable: the DPR presents a negative bias which is not affected by NUBF, but shows increased standard deviation values with larger NUBF; on the other hand, the CMB product bias moves from negative to positive values for NUBF > 0.6, with its standard deviation also increasing with NUBF, and tends to exceed the standard deviation of the DPR product. Kirstetter et al. (2015) found the TRMM PR bias to be dependent upon NUBF effects, whereas this study finds that the GPM DPR bias has virtually no dependency. The reason as to why the GPM DPR bias lacks dependency on NUBF is unclear and highlights the need for further investigations into NUBF effects on radar and radiometer precipitation retrieval algorithms.

f. Misclassification of the clutter-free bottom bin

A plausible reason for explaining part of the rainfall underestimation by GPM products resides in the inaccuracies for the determination of the CFBB in the DPR algorithm. As is seen in Fig. 3, clutter can sometimes be misclassified. This is the case especially in the presence of low freezing levels. In such cases, the DPR algorithm struggles to differentiate between surface clutter and the bright band. The surface rainfall estimates are based on the reflectivity at the CFBB. If a significant part of the DPR profile is not considered, then the usual reflectivity profile issues come into play and rain rates will be underestimated. To understand the extent of this issue, a histogram of the differences between the CFBB altitude and the surface elevation for all quality-controlled and down-selected data at 5-km resolution from within the central five rays of the DPR is plotted in Fig. 12. Range effects are reduced by only considering data from measurements taken within 75 km of a ground-based radar. The plots show that 5.4% of the profiles have a CFBB–surface elevation difference of 1.25 km or more. Furthermore, Fig. 12b
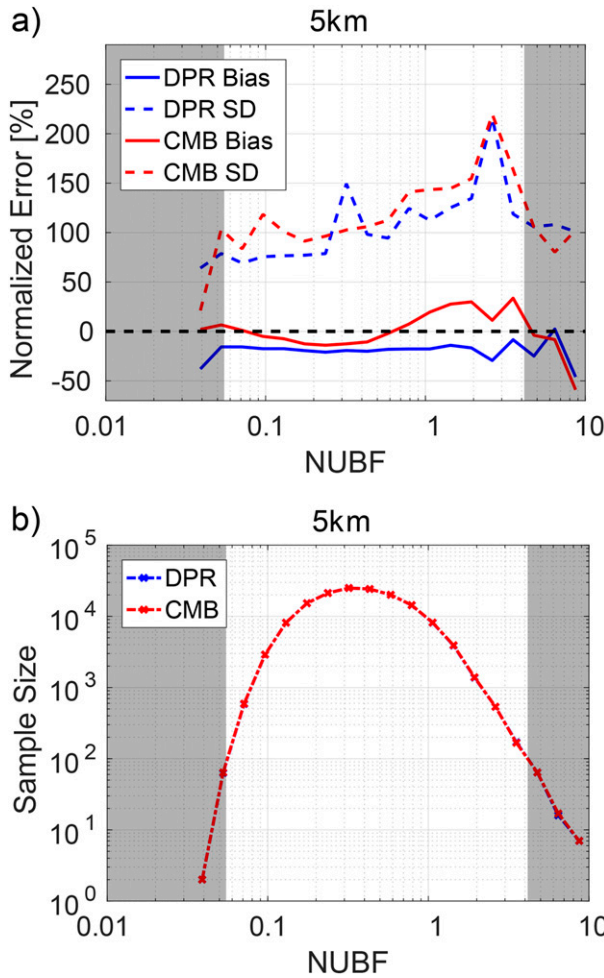
FIG. 11. (a) Bias and SD and (b) sample size of the GPM products with respect to the Radarnet product at 5-km resolution as a function of NUBF factor, using measurements taken within 75 km of a ground-based radar. Sample sizes for the DPR and CMB products are very similar, hence the CMB distribution overlies the DPR distribution. The gray shaded regions represent where there is a sample size of less than 100 pixels.
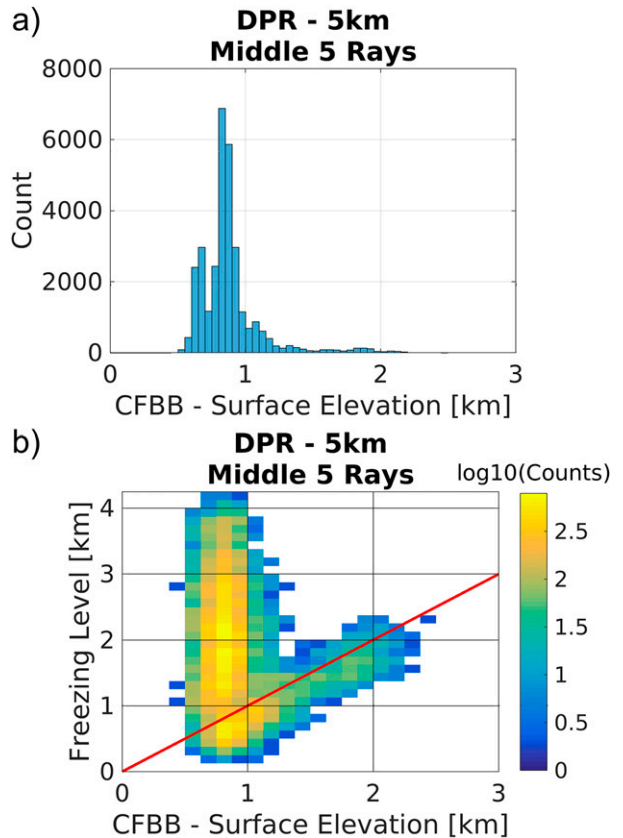

FIG. 12. (a) A histogram of the differences in CFBB altitude and surface elevation at 5-km resolution, using all measurements taken within 75-km range of a ground-based radar from the DPR–Radarnet quality-controlled and down-selected comparison dataset that correspond to the middle five rays of the DPR (to avoid off-nadir effects). (b) A density scatterplot of the same data as a function of the difference in CFBB altitude and surface elevation, and the freezing level altitude. Note that the surface elevation was determined using a combination of the ellipsoid bin offset and surface elevation variables from the DPR product. Other quantities are also from the DPR product.

shows a bimodal distribution between freezing level and CFBB–surface elevation difference. One mode overlying the 1:1 line is related to the clutter detection problem and suggests that the corresponding data are associated with (wrong) attributions of the surface clutter level to the melting level. Considering the dataset used for Fig. 12 with a sample size of 30 826, the bias, standard deviation, and correlation values are −15%, 102%, and 0.60, respectively. Upon removal of the data points with a CFBB–surface elevation difference of 1.25 km or more (new sample size of 29 155), the bias (−11%) and correlation (0.63) were found to improve and the standard deviation (104%) only increased slightly. As such, it appears that misclassification of the

CFBB partially accounts for the underestimation of the DPR product with respect to Radarnet.

4. Conclusions and discussion

This study has compared GPM DPR and CMB (DPR and GMI) version-5 level-2 products to the Radarnet 4 surface rain rate product over GBI during the period from May 2014 to April 2017 at resolutions of 5 and 25 km. The results of the comparison conducted at different spatial resolutions can be summarized as follows:

1) The optimal DPR/CMB detection threshold for precipitation over GBI is $0.38\,\mathrm{mm\,h^{-1}}$ at 5-km resolution and $0.06\,\mathrm{mm\,h^{-1}}$ at 25-km resolution. These thresholds are the result of an optimization

process where the HSS is maximized when using the Radarnet precipitation detection as ground truth. At the DPR native resolution, 86% of GBI precipitation occurrences and 26% of precipitation volumes are missed by the GPM instruments. Issues with detections of low rain intensities are more common in this test bed than in other places (e.g., the United States) due to a predominance of lighter rain over GBI.

2) Overall, the CMB and DPR products underestimate rain rates in comparison to the ground-based Radarnet product. At 5-km resolution, the CMB and DPR products underestimate by 6% and 19%, respectively. At 25-km resolution, the CMB and DPR products underestimate by 21% and 31%, respectively. Though underestimates become larger at 25-km resolution, standard deviation and correlation values significantly improve (see Table 2), meaning that most of the random errors introduced by collocation issues are eliminated at the coarser scale.

3) The GPM products both meet the GPM mission science requirements at 25-km resolution for bias, and almost for standard deviation (Fig. 10). The results are very promising, since these requirements are expected to be met at the coarser 50-km resolution.

4) The GPM products are in better agreement with the Radarnet product in the summer months and worst aligned with it in the winter in the presence of low freezing levels, which increases the difficulty of obtaining surface rainfall rates using spaceborne and ground-based instruments (Fig. 9).

5) The DPR and CMB products exhibit a strong dependence for bias and standard deviation on rain rate intensity at the DPR native resolution, with underestimates above ~0.7 and 1.1 mm h^{-1}, respectively (Fig. 10).

6) NUBF is clearly affecting DPR and CMB products, with increased standard deviations for larger NUBF (by a factor of >1.5 when moving from very homogeneous to very heterogeneous rain fields). For the CMB product, the bias is also NUBF dependent with a tendency of overestimating precipitation in inhomogeneous rain and underestimating it in uniform conditions (Fig. 11).

7) Orographic effects influence the difference in rain rate estimates between the GPM products and the Radarnet product, with generally larger underestimations by the GPM products in mountainous regions of GBI. This implies that either GPM performs worse in mountainous regions than over flatter terrains, or that surface rain rates for mountainous regions are overpredicted by ground-based radars. The results of Speirs et al. (2017) for their GPM validation study over Switzerland support the former possibility.

8) The ground-based GBI radars are less reliable for estimating (and tend to underestimate) surface rain rates beyond around 150 km due to the difficulty in capturing precipitation systems with limited vertical extent (Fig. 8). Definitive conclusions of this study are drawn based only upon measurements within 75-km radius of a ground-based radar. The recommendation of using such measurements applies to ground-based radar satellite validation performed at similar latitudes (50°–60°).

9) The ground-based rainfall estimates at far ranges (beyond around 150 km) corresponding to most of the radars in the Met Office radar network are smaller than those provided by the GPM products. On the other hand, rainfall estimates at far ranges in correspondence to the ground-based radars at the High Moorsley (radar 5 in Fig. 1), Thurnham (radar 14), Predannack (radar 17), and Jersey (radar 18) sites are larger with respect to the GPM products (Fig. 8). This may pinpoint at calibration issues with these radars, but further investigation is needed.

10) Misclassification of the CFBB appears to explain some of the rainfall underestimation by the DPR product with respect to the Radarnet product. Bias and correlation statistics improve upon removal of coincident 5-km measurements with a CFBB–surface elevation difference of more than 1.25 km, when considering measurements from within the central five rays of the DPR to avoid off-nadir geometrical effects. The bias decreases from −15% to −11%, and the correlation increases from 0.60 to 0.63.

The underestimations by the spaceborne version-5 products in comparison to the ground-based product are in agreement with previous studies and are certainly attributable to GPM algorithm deficiencies. For GBI, such deficiencies are the results of a complex interplay between unaccounted orographic effects, seasonal variations in the freezing-level height, NUBF, and misidentification of the CFBB. In particular, the CFBB problem requires further research and improvements in future versions of the GPM algorithms. Discrepancies between the GPM and Radarnet products are more likely to occur in the presence of low freezing levels, so further investigations of the performance of radars and radiometers in such conditions is required.

During the course of the study period, the Met Office was upgrading its ground-based radars to dual-polarization (completed in December 2017). The effects of these upgrades are difficult to disentangle from this

study, and no noticeable improvements are visible with time in Fig. 9. Future investigations could attempt to disentangle these effects by comparing the statistics of pixels close to upgraded radars to the statistics from a bootstrapped random sample of pixels near to radars that were not upgraded at the time. Other future studies will benefit from the upgrade with expected improvements both for the quality control and the quantitative estimation of the Radarnet products. The detection of the hydrometeor type could also be used to exclude profiles from the comparison where the ground-based radars are overshooting rain and looking into the bright band or the snow above it. The results of this paper could be used as a benchmark for assessing the real impact of the dual-polarization upgrade in future studies.

REFERENCES

Beard, K. V., and C. Chuang, 1987: A new model for the equilibrium shape of raindrops. *J. Atmos. Sci.*, **44**, 1509–1524, https://doi.org/10.1175/1520-0469(1987)044<1509:ANMFTE>2.0.CO;2.

Bolen, S. M., and V. Chandrasekar, 2000: Quantitative cross validation of space-based and ground-based radar observations. *J. Appl. Meteor.*, **39**, 2071–2079, https://doi.org/10.1175/1520-0450(2001)040<2071:QCVOSB>2.0.CO;2.

Chen, H., and V. Chandrasekar, 2016: Validation of NASA's Global Precipitation Measurement mission with a high-resolution ground radar network. *URSI Asia-Pacific Radio Science Conf.*, Seoul, South Korea, IEEE, 836–839, https://doi.org/10.1109/URSIAP-RASC.2016.7601343.

Doviak, R. J., and D. S. Zrnić, 1993: *Doppler Radar and Weather Observations*. Courier Corporation, 458 pp.

Fairman, J. G., D. M. Schultz, D. J. Kirshbaum, S. L. Gray, and A. I. Barrett, 2015: A radar-based rainfall climatology of Great Britain and Ireland. *Weather*, **70**, 153–158, https://doi.org/10.1002/wea.2486.

——, ——, ——, ——, and ——, 2017: Climatology of size, shape, and intensity of precipitation features over Great Britain and Ireland. *J. Hydrometeor.*, **18**, 1595–1615, https://doi.org/10.1175/JHM-D-16-0222.1.

Harrison, D. L., S. J. Driscoll, and M. Kitchen, 1998: Improving precipitation estimates from weather radar using quality control and correction techniques. Observation Based Products Tech. Rep. 13, Met Office, 10 pp.

——, K. Norman, C. Pierce, and N. Gaussiat, 2012: Radar products for hydrological applications in the UK. *Proc. Inst. Civ. Eng. Water Manage.*, **165**, 89–103, https://doi.org/10.1680/wama.2012.165.2.89.

——, ——, T. Darlington, D. Adams, N. Husnoo, C. Sandford, and S. Best, 2015: The evolution of the Met Office radar data quality control and product generation system: Radarnet. *37th Conf. Radar Meteorology*, Norman, OK, Amer. Meteor. Soc., 14B.2, https://ams.confex.com/ams/37RADAR/webprogram/Paper275684.html.

Hou, A. Y., and Coauthors, 2014: The Global Precipitation Measurement Mission. *Bull. Amer. Meteor. Soc.*, **95**, 701–722, https://doi.org/10.1175/BAMS-D-13-00164.1.

Iguchi, T., and Coauthors, 2016: Precipitation rates estimated with GPM's Dual-frequency Radar. *2016 IEEE Int. Geoscience and Remote Sensing Symp.*, Beijing, China, IEEE, 3917–3918, https://doi.org/10.1109/IGARSS.2016.7730017.

——, S. Seto, R. Meneghini, N. Yoshida, J. Awaka, M. Le, V. Chandrasekar, and T. Kubota, 2017: GPM/DPR level-2. Algorithm Theoretical Basis Doc., 81 pp., https://pmm.nasa.gov/sites/default/files/document_files/ATBD_DPR_201708_whole_1.pdf.

Kidd, C., J. Tan, P.-E. Kirstetter, and W. A. Petersen, 2018: Validation of the Version 05 Level 2 precipitation products from the GPM Core Observatory and constellation satellite sensors. *Quart. J. Roy. Meteor. Soc.*, https://doi.org/10.1002/qj.3175, in press.

Kirschbaum, D. B., and Coauthors, 2017: NASA's remotely sensed precipitation: A reservoir for applications users. *Bull. Amer. Meteor. Soc.*, **98**, 1169–1184, https://doi.org/10.1175/BAMS-D-15-00296.1.

Kirstetter, P.-E., and Coauthors, 2012: Toward a framework for systematic error modeling of spaceborne precipitation radar with NOAA/NSSL ground radar–based National Mosaic QPE. *J. Hydrometeor.*, **13**, 1285–1300, https://doi.org/10.1175/JHM-D-11-0139.1.

——, Y. Hong, J. Gourley, M. Schwaller, W. Petersen, and J. Zhang, 2013: Comparison of TRMM 2a25 products, version 6 and version 7, with NOAA/NSSL ground radar–based national mosaic QPE. *J. Hydrometeor.*, **14**, 661–669, https://doi.org/10.1175/JHM-D-12-030.1.

——, ——, ——, ——, ——, and Q. Cao, 2015: Impact of sub-pixel rainfall variability on spaceborne precipitation estimation: Evaluating the TRMM 2A25 product. *Quart. J. Roy. Meteor. Soc.*, **141**, 953–966, https://doi.org/10.1002/qj.2416.

Kitchen, M., R. Brown, and A. Davies, 1994: Real-time correction of weather radar data for the effects of bright band, range and orographic growth in widespread precipitation. *Quart. J. Roy. Meteor. Soc.*, **120**, 1231–1254, https://doi.org/10.1002/qj.49712051906.

Marshall, J., W. Hitschfeld, and K. Gunn, 1955: Advances in radar weather. Advances in Geophysics, Vol. 2, Academic Press, 1–56, https://doi.org/10.1016/S0065-2687(08)60310-6.

Meneghini, R., H. Kim, L. Liao, J. A. Jones, and J. M. Kwiatkowski, 2015: An initial assessment of the surface reference technique applied to data from the Dual-Frequency Precipitation Radar (DPR) on the GPM satellite. *J. Atmos. Oceanic Technol.*, **32**, 2281–2296, https://doi.org/10.1175/JTECH-D-15-0044.1.

Met Office, 2003: Met Office rain radar data from the NIMROD system. Subset used: May 2014–April 2017, NCAS British Atmospheric Data Centre, accessed 19 October 2017, http://catalogue.ceda.ac.uk/uuid/82adec1f896af6169112d09cc1174499.

——, 2009: Radar. National Meteorological Library and Archive Fact Sheet 15, 22 pp., https://www.metoffice.gov.uk/binaries/content/assets/mohippo/pdf/j/h/fact_sheet_no._15.pdf.

Mroz, K., A. Battaglia, T. J. Lang, D. J. Cecil, S. Tanelli, and F. Tridon, 2017: Hail-detection algorithm for the GPM *Core Observatory* satellite sensors. *J. Appl. Meteor. Climatol.*, **56**, 1939–1957, https://doi.org/10.1175/JAMC-D-16-0368.1.

NASA, 2014: Precipitation Processing System Global Precipitation Measurement: File specification for GPM products, version 1.08 TKIO 3.60.4. NASA Doc., 1311 pp., https://storm.pps.eosdis.nasa.gov/storm/filespec.GPM.V1.pdf.

——, 2017: GPM 2A-DPR and 2B-CMB, version 5 (V05). Subset used: May 2014 – April 2017, NASA, accessed 23 October 2017, https://pmm.nasa.gov/data-access/downloads/gpm.

Olson W. S., H. Masunaga, and GPM Combined Radar-Radiometer Algorithm Team, 2011: GPM combined radar-radiometer precipitation algorithm theoretical basis document (version 4). 64 pp., https://pmm.nasa.gov/sites/default/files/document_files/Combined_algorithm_ATBD.V04.rev_.pdf.

Simpson, J., C. Kummerow, W.-K. Tao, and R. F. Adler, 1996: On the Tropical Rainfall Measuring Mission (TRMM). *Meteor. Atmos. Phys.*, **60**, 19–36, https://doi.org/10.1007/BF01029783.

Skofronick-Jackson, G., G. Huffman, E. Stocker, and W. Petersen, 2016: Successes with the Global Precipitation Measurement (GPM) mission. *2016 IEEE Int. Geoscience and Remote Sensing Symp.*, Beijing, China, IEEE, 3910–3912, https://doi.org/10.1109/IGARSS.2016.7730015.

——, and Coauthors, 2017: The Global Precipitation Measurement (GPM) mission for science and society. *Bull. Amer. Meteor. Soc.*, **98**, 1679–1695, https://doi.org/10.1175/BAMS-D-15-00306.1.

——, D. Kirschbaum, W. Petersen, G. Huffman, C. Kidd, E. Stocker, and R. Kakar, 2018: The Global Precipitation Measurement (GPM) mission's scientific achievements and societal contributions: Reviewing four years of advanced rain and snow observations. *Quart. J. Roy. Meteor. Soc.*, https://doi.org/10.1002/qj.3313, in press.

Speirs, P., M. Gabella, and A. Berne, 2017: A comparison between the GPM dual-frequency precipitation radar and ground-based radar precipitation rate estimates in the Swiss Alps and Plateau. *J. Hydrometeor.*, **18**, 1247–1269, https://doi.org/10.1175/JHM-D-16-0085.1.

Warren, R. A., 2014: Quasi-stationary convective systems in the UK. Ph.D. thesis, University of Reading, 176 pp.

——, A. Protat, S. T. Siems, H. A. Ramsay, V. Louf, M. J. Manton, and T. A. Kane, 2018: Calibrating ground-based radars against TRMM and GPM. *J. Atmos. Oceanic Technol.*, **35**, 323–346, https://doi.org/10.1175/JTECH-D-17-0128.1.

Wen, Y., Q. Cao, P.-E. Kirstetter, Y. Hong, J. J. Gourley, J. Zhang, G. Zhang, and B. Yong, 2013: Incorporating NASA spaceborne radar data into NOAA National Mosaic QPE system for improved precipitation measurement: A physically based VPR identification and enhancement method. *J. Hydrometeor.*, **14**, 1293–1307, https://doi.org/10.1175/JHM-D-12-0106.1.